Study of clad layer thickness evolution during hot rolling of clad plate with composition S355+316L

A. G. Kolesnikov, *Dr. Eng., Prof.* [1], *e-mail: kolesnikov_ag@bmstu.ru;*
A. G. Zinyagin, *Cand. Eng., Associate Prof.* [1], *e-mail: ziniagin_ag@bmstu.ru;*
A. V. Muntin, *Cand. Eng., Associate Prof.* [1], *e-mail: muntin_av@bmstu.ru*
A. P. Stepanov, *Postgraduate Student* [1], *e-mail: Stepanov_ap@bmstu.ru;*
N. R. Borisenko, *Postgraduate Student* [1], *e-mail: borisenko_nr@bmstu.ru*

[1] *Bauman Moscow State Technical University (Moscow, Russia)*

The article is devoted to the study of the cladding layer thickness evolution during the hot rolling of a S355+316L clad plate. In the production of clad rolled products, the main challenge is the significant non-uniform deformation of the dissimilar layers, leading to an uneven cladding layer thickness, which is regulated by standards. The aim of the work was a comprehensive study of the co-deformation of the layers to analyze the influence of the reduction strategy on the formation of the cladding layer geometry and based on this, to develop practical recommendations. To achieve this goal, an integrated approach was applied, which included determining the rheological properties of the studied steels over a wide range of temperatures and strain rates, as well as developing and subsequent verification of a three-dimensional mathematical model of the rolling process using the finite element method in the ANSYS software package. The model was validated against data from laboratory and industrial experiments, showing an error in predicting the final cladding layer thickness of no more than 7 %. Using the verified model, a numerical study of three different reduction strategies was conducted: a standard one, one with large reductions in the initial passes, and one with small reductions at the beginning of the process. The simulation results showed that the cladding layer thickness is significantly non-uniform along the length and width of the rolled sheet. The relative strain ratio varies from ~1.07 in the central part to 1.25–1.35 at the head and tail ends, leading to a difference in the cladding layer thickness of up to 24 %. It was found that the selected rolling strategies have an insignificant effect on the degree of this non-uniformity. The physical reason for the non-uniformity in the central part is the tensile stresses acting on the cladding layer from the base layer, while at the sheet ends the primary contribution comes from longitudinal metal flow and the “extrusion” effect. Based on the approximation of the shape of the thickenings, the amounts of crop required to meet standard requirements were calculated: ~365 mm from the head and tail ends and ~177 mm from each side edge of the sheet. The data obtained are of significant practical importance for optimizing the production processes of clad rolled products.

Key words: hot rolling, clad rolling, cladding layer, asymmetric rolling, variable gauge, modeling, FEM, stress-strain state, crop shear loss, cutting of rolled products.
DOI: 10.17580/cisisr.2025.02.14

Introduction

In the modern metallurgical industry, bimetallic materials with a 316L stainless steel cladding layer are widely used in the chemical, oil, gas, and energy sectors due to their unique combination of high corrosion resistance and mechanical strength [1–3]. The hot rolling process of such materials on plate mills, where the key mechanical properties of the final product are formed, is of particular interest [4].

The main challenge in the production of clad plates is the non-uniform deformation of the cladding layer and the base layer, caused by significant differences in their mechanical properties. Research shows that during rolling on plate mills, the 316L steel cladding layer can experience significant strain gradients, leading to local thickness reduction, waviness, and even loss of material integrity [5–7]. The rolling of asymmetric clad slabs also leads to longitudinal bending of the rolled plate [8]. These defects significantly degrade the material’s performance and limit its application.

Literature data [9–12] indicate that the non-uniformity of deformation during rolling is determined by a combination of factors:

- Differences in the plastic properties of the layers at working temperatures.
- Conditions of contact friction at the interface and in the deformation zone.
- Geometric parameters of rolling (reduction ratio, thickness ratio of the layers).

This non-uniform deformation, in turn, necessitates selecting the initial cladding layer thickness, calculating the sheet cutting layout considering the resulting thickness variation, and choosing corrective measures for flatness (such as roll speed mismatch, differential cooling of one of the surfaces, etc. [8]).

Study [13] notes that at low reduction ratios (20–35 %), the thickness ratio of the layers has little influence on bending. However, at high reductions (40–50 %), bending intensifies with an increase in the thickness ratio. The best flatness

indicators are achieved with a roll speed ratio of 1.02 and a reduction of 40 %.

In [14], it is shown that the thickness of the cladding layer (Cr13 stainless steel) and the base (Q235 carbon steel) after rolling depends on the reduction ratio. An increase in the reduction leads to a greater thickness difference between the layers.

The work [15] demonstrated that the thickness ratio of the layers after rolling is determined by the initial ratio and the reduction. Modeling shows that the final thickness ratio of the clad sheet slightly increases with increasing reduction but remains close to the initial value due to the material properties. For example, with an initial layer thickness ratio of 0.25, the final value changes insignificantly but becomes slightly higher than the initial one. The model's predictions agree well with experiments, with an error of less than 12 %.

Most existing research is focused either on modeling individual aspects of the clad rolling process or on analyzing the properties of the final rolled product, while a comprehensive study of the cladding layer geometry and the process of its formation is insufficiently covered.

In existing standards (GOST 10885, API 5LD, ASTM A263), the cladding layer thickness is regulated as a range of acceptable thicknesses. This is necessary for several reasons:

- during the manufacture of the final product, the clad steel is subjected to various deformation operations – bending, rolling, pressing;
- significant non-uniformity in the cladding layer thickness can lead to distortion of the product's shape during these processes.

With significant thickness variation, a reduction in load-bearing capacity is possible in certain cross-sections, as the mechanical properties of some stainless steels are lower than those of carbon steels.

For manufacturers of clad steel, it is important to know the distribution of the cladding layer thickness to select the optimal initial cladding layer thickness, as well as to determine the crop amount to reduce the conversion factor and production cost.

Studies [16–18] have investigated the strain ratio between cladding and base layers made of different materials. From the conducted research, it is known that during asymmetric rolling, the thickness of the cladding layer is non-uniform along the length and width, necessitating the development of a production technology that accounts for the requirements regarding cladding layer thickness uniformity.

This article presents experimental and computational studies of the co-deformation of a 316L steel cladding layer and an S355 steel base layer during rolling on a plate mill. The influence of the distribution of the reduction across passes (reduction strategy) on the thickness variation of the cladding layer is analyzed. Furthermore, based on the research data, conclusions are drawn regarding a rational reduction strategy from the standpoint of achieving a uniform cladding layer thickness, along with recommendations for determining the crop amount from both the head and tail ends as well as the side crop. The task of determining the crop amount involves selecting such a "setback" from the edges of the clad sheet that ensures the specified tolerance requirements for the cladding layer thickness are met.

To achieve the stated goal, the following tasks were solved:

1. The rheological properties of the investigated steels were determined over a wide range of strains, strain rates, and temperatures using thermomechanical testing and physical modeling.
2. A mathematical model for the hot rolling of clad plates was developed based on the finite element method (FEM).
3. The model was verified using data from industrial and laboratory rolling cases for the studied product range.
4. Rolling simulations with different deformation strategies were performed (see **Table 1**):

Table 1. Studied reduction strategies

Pass No.	Typical Schedule		High reduction in beginning		Low reduction in beginning	
	Thickness, mm	Reduction, %	Thickness, mm	Reduction, %	Thickness, mm	Reduction, %
1	2	3	4	5	6	7
0	257.0	–	257.0	–	257.0	–
1	216.0	16	218.5	15	239.0	7
2	197.3	9	185.7	15	222.3	7
3	179.8	9	157.8	15	206.7	7
4	161.8	10	134.2	15	192.2	7
5	143.6	11	124.8	7	178.8	7
6	125.3	13	109.8	12	166.3	7
7	110.3	12	96.6	12	154.6	7
8	97.0	12	85.0	12	143.8	7
9	85.4	12	74.8	12	133.7	7
10	75.1	12	65.8	12	124.4	7
11	66.1	12	57.9	12	109.5	12
12	58.2	12	51.0	12	96.3	12
13	51.2	12	44.9	12	84.8	12

1	2	3	4	5	6	7
14	45.1	12	39.5	12	74.6	12
15	39.7	12	34.7	12	65.6	12
16	34.9	12	30.6	12	57.8	12
17	30.7	12	–	–	50.8	12
18	–	–	–	–	44.7	12
19	–	–	–	–	39.4	12
20	–	–	–	–	34.6	12
21	–	–	–	–	30.5	12

- With a high reduction in the first 1–2 passes and uniform reduction thereafter (a typical strategy for rolling clad plates);
- With a low reduction in the first 10 passes;
- With a high reduction in the first 5 passes.

5. Technological recommendations were developed for selecting the reduction strategy and the crop amount to ensure the required uniformity of the cladding layer thickness.

Materials and methods

The study investigated the deformation resistance of S355 and 316L grade steels under various deformation conditions. The chemical composition of these steels is presented in the **Table 2**.

Table 2. Chemical composition of studied steel grades

	C	Si	Mn	Cr	Mo	Ni	Nb	Ti	V
316L	0.02	0.54	1.37	18.6	2.69	11.97	–	–	–
S355	0.11	0.55	1.63	0.03	–	0.01	–	0.005	–

Mathematical models were developed using the Finite Element Method (FEM) in ANSYS, employing eight-node elements for 3D modeling. The model did not assume horizontal symmetry due to the differences in properties between the base and cladding layers, but utilized longitudinal symmetry to reduce computation time.

The material properties for steel grade 316L and the finite element model were defined based on the authors' previous works [16–18]. The properties for steel grade S355 were calculated based on the model presented in [19].

General model parameters (a general view of the model is shown in the **Fig. 1**):

- The model consists of six bodies: a pusher, the workpiece, two tables (before and after the stand), and the top and bottom rolls. All bodies except the workpiece are rigid and are not meshed.
- The workpiece was modeled by meshing the cladding layer with weld seams into 8970 elements.
- The base layer was meshed into 22,500 eight-node elements.
- Boundary conditions were added to account for gravity.
- Friction in the model was defined according to Siebel's law [20–26].

To obtain the initial temperature field of the strip, a holding time of 70 s was simulated, corresponding to the average transportation time of the slab from the furnace to the rolling stand. To determine the initial temperature of the workpiece before the finishing passes, a holding period was simulated in accordance with the experimental data.

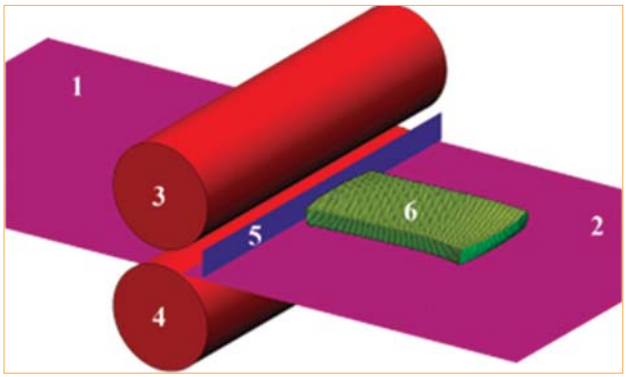

Fig. 1. General view of the model: *1* – front table rolls, *2* – rear table rolls, *3* – top work roll, *4* – bottom work roll, *5* – pusher, *6* – clad slab

The thermal properties of the materials were defined as a function of temperature at the element nodes and in accordance with data from [27].

The relationship between stress and strain in the strip material was defined using an elastic-plastic material behavior model. The plastic properties were assigned based on data obtained from the Gleeble system. The elastic modulus was set as constant and equal to 5×10^{10} Pa. Poisson's ratio was taken as 0.3.

The shape of the cladding layer after rolling was investigated in the front, rear, middle, and side sections. The study zones are schematically shown in the **Fig. 2**.

Model validation

The model was verified against laboratory and industrial experiments previously conducted by the authors and described in detail in [19].

Laboratory samples with a total thickness of 73.5 mm, a cladding layer thickness of 14.8 mm, a width of 100 mm, and a length of 200 mm were rolled according to five regimes listed in **Table 3**. The base layer was made of steel grade 09G2S, and the cladding layer was made of 316L.

The following values for the cladding layer thickness at the center of the samples were obtained (**Table 4**) the industrial case, a strategy analogous to the one designated as "standard" in Table 1 was used. The initial workpiece thick-

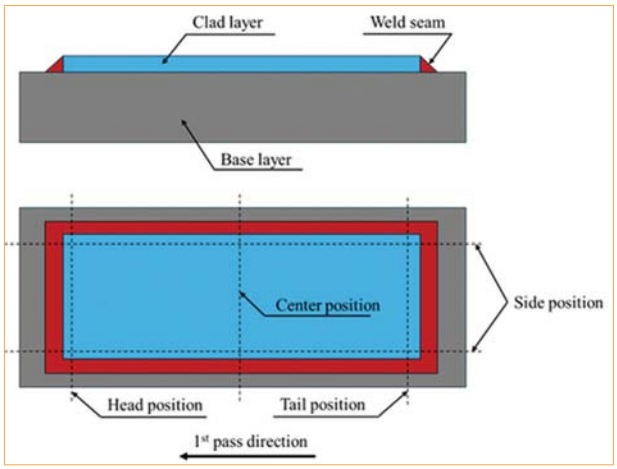

Fig. 2. Investigation points for the shape and thickness of the cladding layer

ness was 257 mm, with a cladding layer thickness of 35 mm. The base layer was made of pipe steel grade with a strength class of K60, and the cladding layer was made of 316L. The simulation resulted in a cladding layer thickness of 3.44 mm, while the industrial sample measured 3.5 mm.

On average, the error in determining the thickness of the cladding layer was 3.4%, with a minimum error of 2.5% and a maximum of 7%. This accuracy is considered sufficient for assessing the influence of the main rolling process parameters on the deformation of the cladding layer in an industrial setting.

Modelling results

To solve the main task – determining the strain ratio of the base and cladding layers – let us introduce the concept of relative strain. This is defined as the ratio of the relative thickness of the cladding layer at the start of deformation to the relative thickness of the cladding layer at the end of deformation:

$$\vartheta = \frac{H_{tot.init}}{h_{clad.init}} \div \frac{H_{tot.i}}{h_{clad.i}} \quad (1)$$

where $H_{tot.init}$, $h_{clad.init}$ are the initial total thickness and initial cladding layer thickness $H_{tot.i}$, is the total thickness of the rolled product in the i-th pass, $h_{clad.i}$ is the cladding layer thickness in the i-th pass.

The total logarithmic strain is adopted as the argument for analyzing the co-deformation of the base and cladding layers:

$$\lambda = ln\frac{H_{tot.init}}{H_{tot.i}} \quad (2)$$

Fig. 3 shows the dependence of the relative strain coefficient on the total logarithmic strain for the three considered strategies in the front, rear, and side sections of the rolled product.

The fluctuations in the calculated values are caused by inaccuracies in both the direct calculation of the cladding layer thickness and the finite element method (FEM) calculation due to variations in the peak position resulting from the discrete nature of the process (different entry conditions into the deformation zone caused by the time step).

As can be seen from Fig. 3, the mutual deformation coefficient increases sharply in the first 2–3 passes for all investigated positions. Subsequently, for the central position, it increases very slowly from 1.035 to 1.074 (on average for the three strategies). For the front, rear, and side parts, a more pronounced increase to values of 1.25–1.35 is characteristic, with a lower value for the side part.

In the central part during the initial passes, there is a possibility of the less strong base layer (S355 steel) being "extruded" by the stronger cladding layer, which forms the main

Table 3. Rolling regimes on the laboratory mill

Pass	1			2			3			4		
No.	t,°C	h, mm	ε, %	t,°C	h, mm	ε, %	t,°C	h, mm	ε, %	t,°C	h, mm	ε, %
1	1200	56.7	23	1200	57.0	22	1200	57.0	22	1200	57.0	23
2	–	43.9	23	–	43.9	23	–	43.9	23	–	43.9	23
3	956	34.0	23	942	37.3	15	931	34.0	23	928	34.0	23
4	–	26.0	23	–	31.7	15	–	27.7	19		27.7	19
5	–	20.0	23	–	27.0	15	–	23.4	16	882	23.4	16
6	908	15.6	23	–	22.9	15	–	20.3	13	–	–	–
7	–	–	–	–	19.5	15	855	17.9	12	–	–	–
8	–	–	–	–	16.5	15	–	–	–	–	–	–
9	–	–	–	–	14.0	15	–	–	–	–	–	–
10	–	–	–	795	12.0	14	–	–	–	–	–	–

Table 4. Comparison of simulation results and laboratory experiments

Sample №	Calculated Clad layer final thickness, mm	Measured Clad layer final thickness, mm
1	4.84	4.90
2	4.10	4.00
3.4	5.51 – 5.58	5.60
5	7.05	7.10

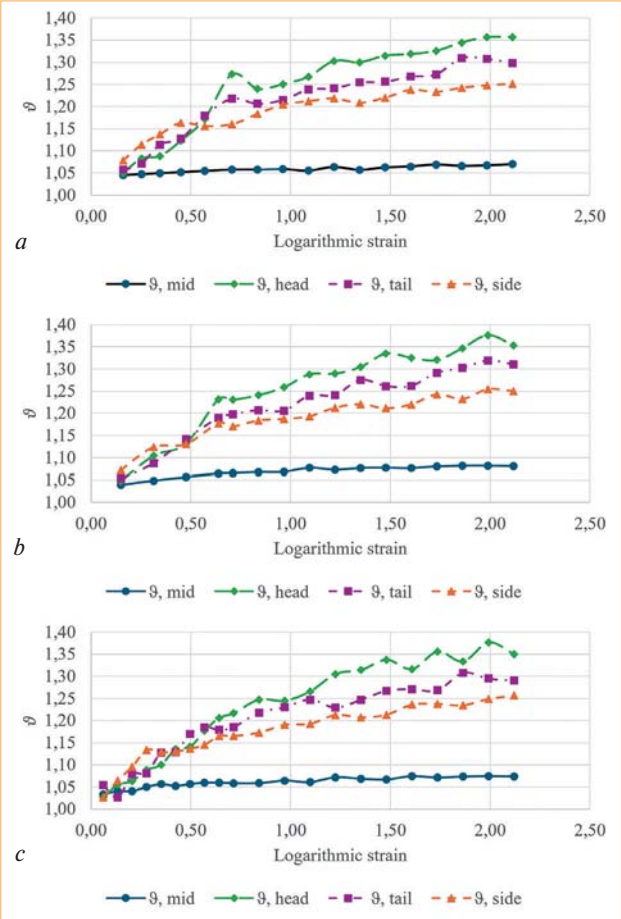

Fig. 3. Dependence of the mutual deformation coefficient for the standard reduction strategy (*a* – standard strategy, *b* – large reductions, *c* – small reductions)

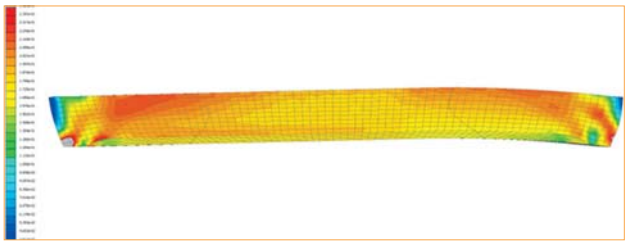

Fig. 4. Distribution of the total plastic strain after one pass

non-uniformity of deformation. This effect manifests itself in the following ways:

- The cladding layer is "indented" into the base layer as the surface area of the rolled product increases due to the underlying layers of the base layer reaching the contact surface with the rolls.
- The formation of a bend in the rolled product (i.e., the base layer experiences greater elongation).

During subsequent deformation, the cladding layer deforms almost identically to the base layer due to the action of frictional forces on the surface of the rolled product from contact with the rolls. These forces prevent the metal from flowing freely and thus prevent greater deformation of the stronger layer. The deformation of the cladding layer occurs due to the action of tensile stresses from the base layer.

Fig. 4 shows the distribution of the total plastic strain after the second pass using the standard strategy. It is evident that the cladding layer is more heavily deformed in the center than at the head and tail ends, while in the center, the deformation of the base and cladding layers is similar.

Fig. 5 shows a comparison of the stresses arising in the central and front parts of the workpiece. The images *a, b* display equivalent stresses in the central and front parts; a lower average stress in the front part can be noted, related to the reasons described above – the stronger cladding layer "extrudes" the material of the base layer towards the front end of the workpiece. The images *c, d* show stresses along the Oy axis which are distributed similarly through the deformation zone for the two positions, with larger values for the central position. The images *e, f*) show stresses along the Ox axis. Larger values in the central section are evident.

For the front and rear parts, as well as for the middle part, there exists the possibility of the less strong base layer (S355 steel) being "extruded" by the stronger cladding layer due to the elongation of the base layer and the transition of deeper layers to the contact surface with the rolls. This effect is observed from pass to pass with gradual attenuation. Due to the different stress-strain state in the first pass, the front part of the cladding layer receives less deformation than the rear part, and this difference persists until the end of the rolling process.

Fig. 6 shows the variation of stresses along the Ox axis for the front and middle sections during the rolling process. The

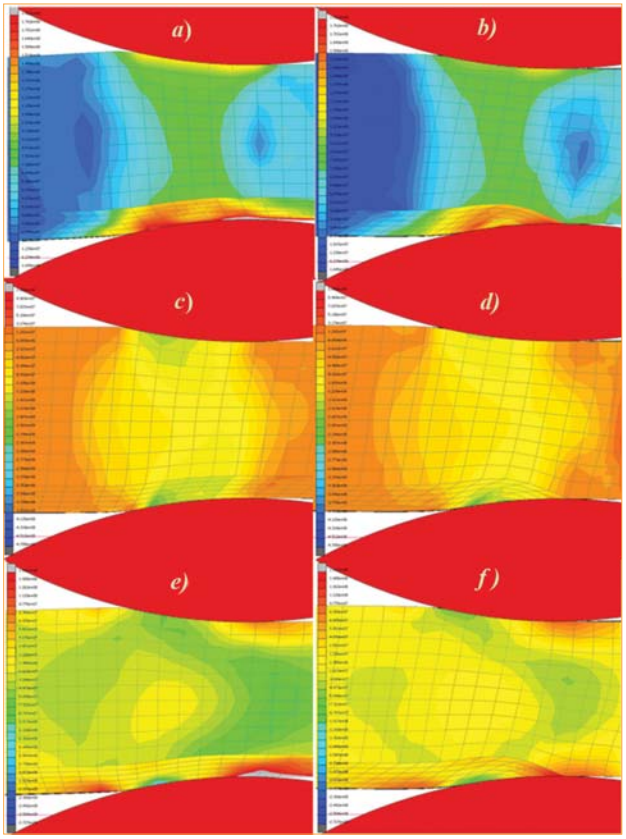

Fig. 5. Distribution of equivalent stresses for the central and front positions (*a, b*)**, distribution of stresses along the Oy axis** (*c, d*) **and along the Ox axis** (*e, f*)

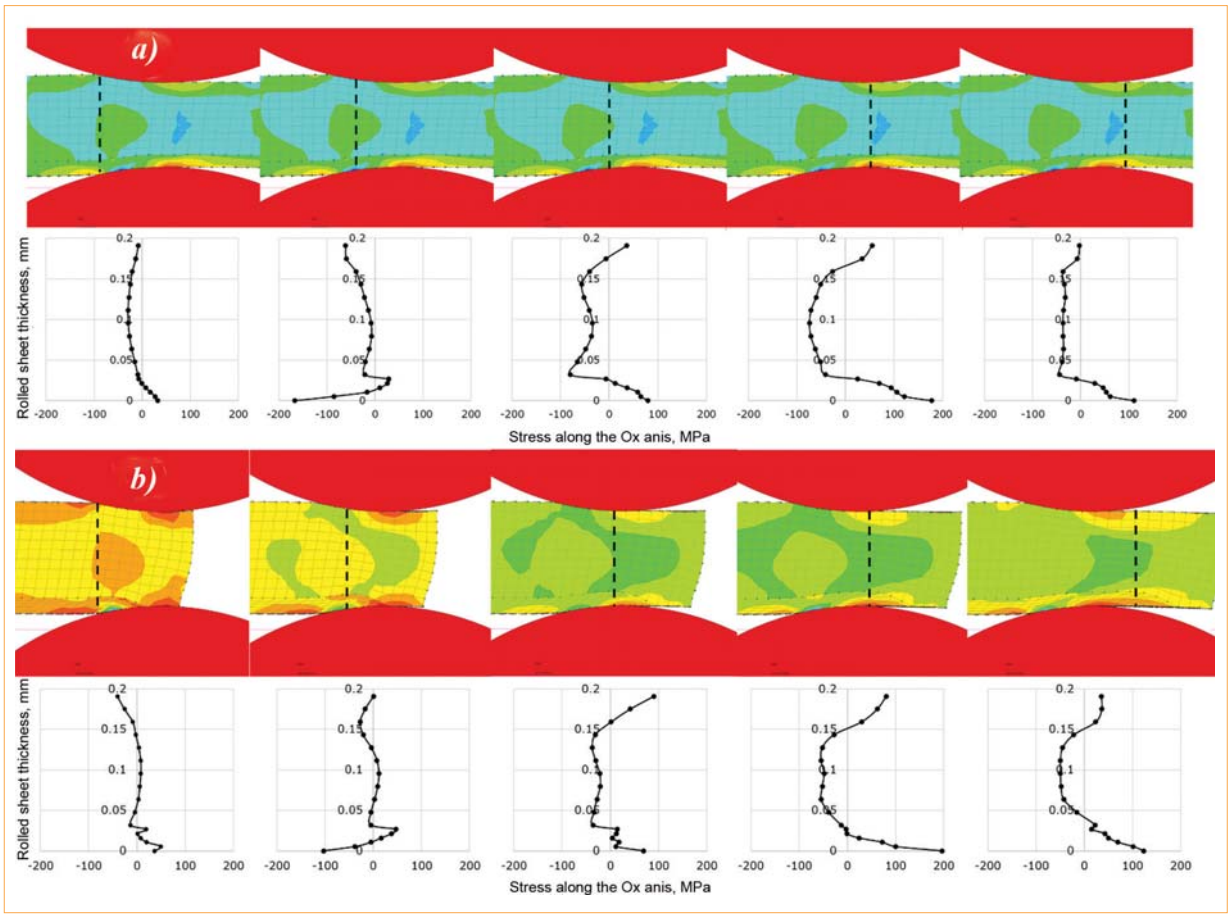

Fig. 6. Variation of stresses along the Ox axis for the middle section (*a*) and variation of stresses along the Ox axis for the front section (*b*)

general character of the stress variation is similar for both positions; however, larger tensile stresses can be noted for the middle section – the average value of tensile stresses (at the position where stresses are maximum) in the cladding layer is 42 % greater (81 MPa compared to 57 MPa in the front part), which explains the greater deformation of the cladding layer in the middle. For the rear part of the rolled product, the ratio of tensile stresses to the middle part is analogous.

Comparing the different strategies, minor differences in the relative strain coefficients can be noted across all investigated sections. The maximum value of the coefficient 9 in the central section is the highest (1.084) for the strategy with large reductions and the lowest for the strategy with smaller reductions (1.069). Given initial thicknesses of the base and cladding layers of 229 mm and 35 mm respectively, this difference translates to a difference in the final cladding layer thickness of 0.05 mm – 4.49 mm and 4.54 mm respectively, or 1%. For the front, rear, and side parts, the difference in coefficients is even smaller and can be attributed to simulation error.

For the head and tail ends, the coefficients range from 1.29 to 1.35, which corresponds to a cladding layer thickness of 5.42–5.67 mm. The difference in thickness between the front, rear, and middle parts is more than 1.1 mm or 24%.

In practice, a safety margin is always used when calculating the final cladding layer thickness, typically around +10 %. Considering the maximum calculated non-uniformity of 24 %, the total excess of the cladding layer thickness over the target value can reach up to 34 %, which is significantly higher than the allowable limit (approximately 25 % according to GOST 10885).

The conducted modeling revealed the following lengths of the thickened sections of the cladding layer, **Fig. 7** schematically shows a cross-section indicating the shape of the cladding layer at the edge of the strip. Length l_1 is the total length of the thickened zone, l_2 is the distance from the edge of the cladding layer to the point where its thickness reaches a permissible value, and l_3 is the location of the maximum cladding layer thickness.

The simulation yielded the following values for the lengths of the thickened sections of the cladding layer, see

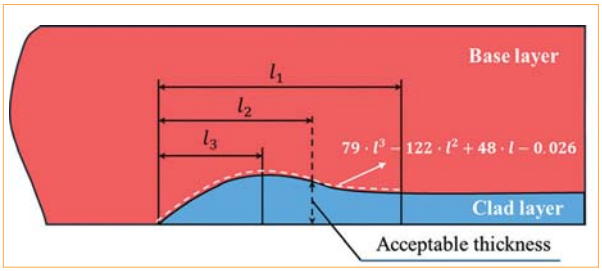

Fig. 7. Description of the cladding layer shape

Table 5. Parameters of cladding layer thickness non-uniformity at the head and tail ends

No.	Thickness, mm	Log. Strain	l_1, mm	l_3,mm
0	254.0	0	0	0
1	216.0	0.16	90.3	163.1
2	197.3	0.25	95.9	173.1
3	179.8	0.35	102.7	186.8
4	161.8	0.45	107.9	197.5
5	143.6	0.57	119.1	218.8
6	125.3	0.71	124.5	234.5
7	110.3	0.83	134.0	252.5
8	97.0	0.96	143.0	270.0
9	85.4	1.09	152.6	285.5
10	75.1	1.22	159.2	300.9
11	66.1	1.35	166.8	316.3
12	58.2	1.47	173.6	332.7
13	51.2	1.60	182.6	350.2
14	45.1	1.73	193.3	370.5
15	39.7	1.86	200.4	384.1
16	34.9	1.98	206.7	415.4
17	30.7	2.11	216.8	422.6

Table 5 (values for the standard strategy are shown, as they were similar to the other cases, much like the layer thickness values).

The shape of the cladding layer at the head and tail ends is described by a third-order curve:

$$th = 121.99 \cdot l^3 - 149.62 \cdot l^2 + 52.001 \cdot l - 0.0825 \quad (3)$$

where th – clad layer thickness, l – distance from the beginning of clad layer.

Considering that the allowable excess thickness of the cladding layer, taking into account the existing margin, results in an additional possible excess of 0.45 mm, which, according to equation (3), necessitates cropping 365 mm of the cladding layer.

For the side section, the values of l_1 and l_3 remain practically unchanged after the third pass and are equal to 120 mm and 201 mm, respectively. The formula for describing the shape of the irregularity is:

$$th = 395.86 \cdot l^3 - 391.23 \cdot l^2 + 84.941 \cdot l - 0.0593 \quad (4)$$

In a similar formulation, 177 mm must be trimmed off.

Conclusions

1. A 3D finite element model of the hot rolling process for bimetallic sheet has been developed and verified, adequately describing the co-deformation of the dissimilar layers. The model's error in predicting the final cladding layer thickness does not exceed 7 % compared to laboratory and industrial data.

2. It has been established that the cladding layer thickness is non-uniform along the length and width of the rolled sheet. The relative strain coefficient (ϑ) varies from ~1.07 in the central part to 1.25–1.35 at the head and tail ends, leading to a difference in cladding layer thickness of up to 24 %.

3. It has been demonstrated that the three investigated rolling strategies (standard, with high initial reductions, with low initial reductions) have an insignificant influence on the degree of cladding layer thickness non-uniformity. The maximum difference in the final thickness in the central part was only about 1 %.

4. The physical causes of the non-uniformity have been identified:

- In the central part, the primary mechanism is the tensile stresses acting on the cladding layer from the base layer during its deformation.
- At the head and tail ends, the main contribution comes from longitudinal metal flow: the stronger cladding layer (316L) hinders deformation, while the base layer elongates due to bending and the movement of deeper layers to the surface, leading to significant thickening of the cladding layer ends.
- Analysis of the stress state confirmed that the tensile stresses in the cladding layer in the central part are 42 % higher than at the ends, explaining its greater deformation in the middle of the sheet.

5. Considering the standard margin for cladding layer thickness (~10 %) and the identified non-uniformity (up to +24 %), the total thickness excess can reach 34%, which is unacceptable for most standards.

6. Based on the approximation of the thickening shapes, it has been calculated that for the investigated combination of thicknesses and steel grades of the clad product, compensating for the non-uniformity requires cropping the cladding layer:

- ~365 mm from the head and tail ends of the sheet.
- ~177 mm from each side edge of the sheet.

REFERENCES

1. Cho Y.-R. Clad Metals: Fabrication, Properties, and Applications. *Metals*. 2021. No. 11. 1186. DOI: 10.3390/met11081186.
2. Giudice F., Missori S., Scolaro C., Sili A. A Review on Metallurgical Issues in the Production and Welding Processes of Clad Steels. *Materials*. 2024. Vol. 17. 4420. DOI: 10.3390/ma17174420.
3. Wang D., Sun X., Jiang Y., Chang X., Yonglei X. Review on the application of stainless-clad bimetallic steel in the marine environment. *Anti-Corros. Methods Mater*. 2024. Vol. 71. pp. 132–142.
4. Jiang J., Ding H., Lu Z., Xie G. Interfacial microstructure and mechanical properties of stainless steel clad plate prepared by vacuum hot rolling. *J. Iron Steel Res. Int*. 2018. Vol. 25. pp. 732–738.
5. Jin H. R., Wei R., Wang Y. H. et al. Vacuum Hot Rolling Preparation of a Stainless Steel Clad Plate and Its Numerical Simulation. *Strength Mater*. 2022. Vol. 54. pp. 144–153. DOI: 10.1007/s11223-022-00388-1.
6. Guan B., Chen B. Y., Zang Y. et al. Prediction of a High Temperature Bonding Condition at the Interface for the Hot-Rolled Stainless Steel Clad Plate on Rolling. *Strength Mater*. 2018. Vol. 50. pp. 79–91. DOI: 10.1007/s11223-018-9945-1.
7. Jin H. R., Zhang L., Dai C. et al. Numerical Simulation and Experimental Study on the Interface Bonding of Stainless Steel Clad Plate. *Strength Mater*. 2018. Vol. 50. pp. 29–40. DOI: 10.1007/s11223-018-9939-z.
8. Zinyagin A. G., Borisenko N. R., Stepanov A. P., Kryuchkova M. O. Development of measures to reduce longitudinal bending of thick clad and alloyed steel plates during hot rolling. *CIS Iron and Steel Review*. 2025. Vol. 29. pp. 56–60.
9. Liu B. X., An Q., Yin F. X. et al. Interface formation and bonding mechanisms of hot-rolled stainless steel clad plate. *J. Mater.*

Sci. 2019. Vol. 54. pp. 11357–11377. DOI: 10.1007/s10853-019-03581-x.
10. Xie G. et al. Interface characteristic and properties of stainless steel/HSLA steel clad plate by vacuum rolling cladding. *Materials Transactions*. 2011. Vol. 52. pp. 1709–1712.
11. Qin Q., Wu Z. H., Zang Y., Guan B., Zhang J. Warping deformation of 316l/q345r stainless composite plate after removal strake. *World journal of engineering*. 2016. Vol. 13 (3). pp. 206–209.
12. Qin Q., Zhang D. T., Zang Y., Guan B. A simulation study on the multi-pass rolling bond of 316L/Q345R stainless clad plate. *Advances in Mechanical Engineering*. 2015. Vol. 7 (7). 1687814015594313.
13. Sun L., Ding J., Zhang J., Li H., Wang G. Numerical Simulation and Deformation Behavior of a Ti/Steel Clad Plate during the Rolling. Process. *Metals*. 2023. Vol. 13. 218. DOI: 10.3390/met13020218.
14. Lian-Yun Jiang, Zhi-Wei Xue, Fu-Zhen Qiao, Qi-Qi Ma, Zhi-Quan Huang, Li-Feng Ma. Modeling and analysis of deformation characteristics for the two-layered metal clad plate produced by asymmetric rolling. *Journal of Materials Research and Technology*. 2023. Vol. 27. pp. 2031–2051. DOI: 10.1016/j.jmrt.2023.10.044.
15. Lian-Yun Jiang, Ya-Fei Chen, Jia-Le Liang, Zhen-Lei Li, Tao Wang, Li-Feng Ma, Modeling of layer thickness and strain for the two-layered metal clad plate rolling with the different roll diameters. *Journal of Materials Research and Technology*. 2024. Vol. 28. pp. 3849–3864. DOI: 10.1016/j.jmrt.2023.12.257.
16. Zinyagin A. G., Muntin A. V., Stepanov A. P., Borisenko N. R. Study of the features of clad sheet deformation during hot rolling. *Chernye Metally*. 2023. No. 12. pp 49–55.
17. Zinyagin A. G., Borisenko N. R., Muntin A. V., Kruychkova M. O. Features of finite element modeling for hot rolling process of clad sheets and strips. *CIS Iron and Steel Review*. 2023. Vol. 26. pp. 51–57.
18. Kolesnikov A. G., Zinyagin A. G., Muntin A. V., Dunaev V. V. Study of joint hot deformation of nickel alloy and low carbon microalloyed steel in manufacture of heavy plate clad rolled products. *CIS Iron and Steel Review*. 2022. Vol. 24. pp. 41–48.
19. Zinyagin A. G., Muntin A. V., Tynchenko V. S., Zhikharev P. I., Borisenko N. R., Malashin I. Recurrent Neural Network (RNN)-Based Approach to Predict Mean Flow Stress in Industrial Rolling. *Metals*. 2024. Vol. 14 (12). p. 1329. DOI: 10.3390/met14121329.
20. Da-Wei Zhang, Fang-Fang Xu, Zai-Chi Yu, Kun-Yin Lu, Ze-Bang Zheng, Sheng-Dun Zhao. Coulomb, Tresca and Coulomb-Tresca friction models used in analytical analysis for rolling process of external spline. *Journal of Materials Processing Technology*. 2021. Vol. 292. p. 117059. DOI: 10.1016/j.jmatprotec.2021.117059.
21. Murillo-Marrodán A., Garcia E., Cortés F. Friction Modelling of a Hot Rolling Process by means of the Finite Element Method. *Proceedings of the World Congress on Engineering 2017 (WCE 2017). July 5–7, 2017*. Vol. II. 2017. London, U.K.
22. Peng L., Lai X., Lee H. J., Song J. H., Ni J. Friction behavior modeling and analysis in micro/meso scale metal forming process. *Mater. Des*. 2010. Vol. 31. pp. 1953–1961.
23. Sverdlik M., Pesin A., Pustovoytov D., Perekhozhikh A. Numerical Research of Shear Strain in an Extreme Case of Asymmetric Rolling. *Advanced Materials Research*. 2013. Vol. 742. pp. 476–481.
24. Graça A., Vincze G. A Short Review on the Finite Element Method for Asymmetric Rolling Processes. *Metals*. 2021. No. 11. p. 762. DOI: 10.3390/met11050762.
25. Pustovoytov D., Pesin A., Biryukova O. Finite element analysis of strain gradients in aluminium alloy sheets processed by asymmetric rolling. *Procedia Manuf*. 2018. Vol. 15. pp. 129–136.
26. Nielsen C. V., Bay N. Overview of friction modelling in metal forming processes. *Procedia Eng*. 2017. Vol. 207. pp. 2257–2262.
27. Philip D. Harvey. Engineering Properties of Steel. American Society for Metals, 1982. p. 527.